The ^{10}B(^{7}Be, ^{8}B)^{9}Be Reaction and the ^{7}Be$(p,\gamma)^{8}$B S Factor

A. Azhari,[1] V. Burjan,[2] F. Carstoiu,[3] H. Dejbakhsh,[1] C. A. Gagliardi,[1] V. Kroha,[2] A. M. Mukhamedzhanov,[1] L. Trache,[1] and R. E. Tribble[1]

[1]*Cyclotron Institute, Texas A&M University, College Station, Texas 77843*
[2]*Institute for Nuclear Physics, Czech Academy of Sciences, Prague-Řež, Czech Republic*
[3]*Institute of Physics and Nuclear Engineering, Bucharest, Romania*

(Received 23 December 1998; revised manuscript received 24 February 1999)

The ^{10}B(^{7}Be, ^{8}B)^{9}Be reaction has been studied with an 84 MeV ^{7}Be radioactive beam. The measured cross section determines the asymptotic normalization coefficients for the virtual transitions $^{7}\mathrm{Be} + p \leftrightarrow {}^{8}\mathrm{B}$. These coefficients specify the amplitude of the tail of the ^{8}B wave function in the two-body channel $^{7}\mathrm{Be} + p$, and may be used to calculate the S factor for the direct capture reaction $^{7}\mathrm{Be}(p,\gamma)^{8}\mathrm{B}$ at solar energies, $S_{17}(0)$. We find that $S_{17}(0) = 17.8 \pm 2.8$ eV b. [S0031-9007(99)09160-7]

PACS numbers: 25.60.Je, 25.60.Bx, 26.65.+t, 26.20.+f

^{8}B produced via the $^{7}\mathrm{Be}(p,\gamma)^{8}\mathrm{B}$ reaction is the source of most or, in some cases, all solar neutrinos observed in several existing and planned solar neutrino experiments (e.g., Homestake, Kamiokande, Super-Kamiokande, SNO). Thus, the cross section for the $^{7}\mathrm{Be}(p,\gamma)^{8}\mathrm{B}$ reaction at solar energies ($\sim$20 keV), or equivalently its S factor $S_{17}(0)$, plays a crucial role in the solar neutrino question. There have been five direct measurements of this cross section using radioactive ^{7}Be targets with uncertainties less than 20%. When the measured S factors are extrapolated from the observed energy ranges down to $E_{\mathrm{c.m.}} = 0$, each experiment gives a determination of $S_{17}(0)$ to $\approx$10%, but two of the results [1,2] are near 25 eV b, while the other three [3–5] are near 18 eV b. All experiments are consistent with the predicted energy dependence of $S(E)$ [6–8], indicating this discrepancy is due to unresolved problems in absolute normalizations. Therefore, the most recent review of solar fusion rates adopted a value $S_{17}(0) = 19^{+4}_{-2}$ eV b [9], making $S_{17}(0)$ the most uncertain input for solar model calculations. This review also emphasized the importance of additional indirect determinations of $S_{17}(0)$ which are sensitive to different systematic effects from those present in the direct cross section measurements. One indirect determination has been performed, based on Coulomb dissociation of ^{8}B [10], and favors the lower values of $S_{17}(0)$. But the reliability of Coulomb dissociation to determine astrophysical S factors at stellar energies has not yet been verified [9].

In this Letter, we report the first indirect measurement of the $^{7}\mathrm{Be}(p,\gamma)^{8}\mathrm{B}$ capture rate at solar energies via a determination of the asymptotic normalization coefficient (ANC) for $^{7}\mathrm{Be} + p \leftrightarrow {}^{8}\mathrm{B}$, as proposed in [6]. At solar energies, the $^{7}\mathrm{Be}(p,\gamma)^{8}\mathrm{B}$ capture proceeds through the tail of the nuclear overlap function [6]. The shape of this tail is determined by the Coulomb interaction, so the capture rate can be calculated accurately if one knows its amplitude. The asymptotic normalization coefficients for $^{7}\mathrm{Be} + p \leftrightarrow {}^{8}\mathrm{B}$ specify the amplitude of the tail of the ^{8}B wave function in the two-body channel when the ^{7}Be core and the proton are separated by a distance large compared to the nuclear radius.

The advantage of the ANC approach is that it provides a method to determine direct capture S factors at zero energy from measurements of nuclear reactions, such as peripheral nucleon transfer, which have cross sections orders of magnitude larger than the direct capture reactions themselves. In a previous study [11], we tested this technique by comparing measured S factors for $^{16}\mathrm{O}(p,\gamma)^{17}\mathrm{F}$ with calculations based on ANC's measured in the peripheral proton transfer reaction $^{16}\mathrm{O}(^{3}\mathrm{He}, d)^{17}\mathrm{F}$. This system is very similar to $^{7}\mathrm{Be}(p,\gamma)^{8}\mathrm{B}$, because they both involve proton capture at large radii into very weakly bound states. The agreement between the $^{16}\mathrm{O}(p,\gamma)^{17}\mathrm{F}$ results based on the measured S factors and those inferred from the measured ANC's was better than 9%. In the present case, we determine the ANC's for the system $^{7}\mathrm{Be} + p \leftrightarrow {}^{8}\mathrm{B}$ from a study of the reaction $^{10}\mathrm{B}(^{7}\mathrm{Be}, {}^{8}\mathrm{B})^{9}\mathrm{Be}$. One previous experiment attempted to measure the ANC's for $^{7}\mathrm{Be} + p \leftrightarrow {}^{8}\mathrm{B}$ with the reaction $^{2}\mathrm{H}(^{7}\mathrm{Be}, {}^{8}\mathrm{B})n$ [12]. However, interpretation of that experiment was complicated by uncertainties in the choice of optical model parameters [13].

The ^{7}Be radioactive beam was produced in the reaction $^{1}\mathrm{H}(^{7}\mathrm{Li}, {}^{7}\mathrm{Be})n$, using a 135 MeV ^{7}Li beam from the Texas A&M University K500 superconducting cyclotron irradiating a 2.8 mg/cm^2 thick LN_2-cooled cryogenic H_2 gas cell with Havar windows. An Al degrader reduced the ^{7}Li beam energy before entering the H_2 gas. 84 MeV ^{7}Be recoils produced at 0° entered the Texas A&M momentum achromat recoil spectrometer (MARS) [14,15], which separated them from the primary beam and other reaction products. Slits distributed through MARS controlled the ^{7}Be beam size and energy and angular spread. The target and beam study detector shown in Fig. 1 were located at the MARS focal plane. The study detector was a 5×5 cm^2, 1000-μm thick, two-dimensional position-sensitive Si detector mounted on the target ladder. The ^{7}Be beam spot was 3 mm horizontal by 6 mm vertical (both FWHM), with an angular spread of 4° horizontal by 1.6°

 0031-9007/99/82(20)/3960(4)$15.00

vertical (full widths) and an energy spread of 1.6 MeV (FWHM). 99.5% of the beam particles were ^{7}Be, with the rest being lower energy α particles. The beam study detector calibrated the ^{7}Be yield, which was typically $\sim$60 kHz, relative to the measured ^{7}Li beam current at the MARS Faraday cup. The ^{7}Be beam intensity, shape, and location were checked frequently and found to be very stable.

The self-supporting ^{10}B target was produced by drying a slurry containing grains of enriched ^{10}B in a varnish on a Ta foil. The ^{10}B layer was removed from the Ta with distilled water. The properties of the target were determined directly by the ^{7}Be beam. One of the two reaction detector assemblies described below was used to compare the energy of the beam through a blank target holder and through the target foil. From the dE/dx measurement, the average thickness of the ^{10}B target was determined to be 1.96 mg/cm^2. The increased energy spread of the beam when passing through the target indicated that it had a significant thickness variation ($\pm$1.3 mg/cm^2) due to the grain size used in the slurry. Since all beam parameters except intensity were kept the same during these measurements as during the actual data collection, the uncertainty in the final result due to the nonuniformity of the target is minimal. Based on auxiliary reaction studies at the Institute for Nuclear Physics, the target was found to contain 77% ^{10}B, with ^{1}H, ^{11}B, ^{12}C, and ^{16}O also present.

Both ^{7}Be elastic scattering and ^{8}B produced in the reaction ^{10}B(^{7}Be, ^{8}B)^{9}Be were observed simultaneously by the reaction telescopes shown in Fig. 1. The telescopes consisted of 5 $\times$ 5 cm^2, 105-μm thick Si ΔE detectors, backed by 1000-μm thick Si E detectors. The ΔE detectors included read-outs from 16 separate resistive strips to provide two-dimensional position information for each event, together with an independent read-out of the energy loss. $\Delta E - E$ particle identification was straightforward. Two different configurations were used for the reaction telescopes. In the first, shown in Fig. 1, they were mounted symmetrically above and below the ^{7}Be beam. In the second configuration, a single telescope was mounted at 0°, a beam stop was attached to block the primary ^{7}Be beam, and slits in MARS were adjusted to reduce the angular and energy spread of the ^{7}Be beam.

^{7}Be elastic scattering data were used to validate our understanding of the beam and detector properties, our choice of optical model parameters, and the determination of the average target thickness. A detailed Monte Carlo simulation of the experiment included all of the measured properties of the beam, energy loss and straggling in the target, the reaction kinematics, and the finite resolution of the detectors. It calculated the solid angle of the detectors as a function of the scattering angle and the overall energy and angular resolutions. Elastic scattering yields were obtained from the data using ^{7}Be events which were kinematically reconstructed by the analysis code based on the assumption that all events resulted from scattering off of ^{10}B nuclei. Figure 2 shows the resulting elastic scattering angular distribution using the solid angle factors obtained from the Monte Carlo simulation. In order to compare the measured angular distribution to optical model predictions, it was necessary to include the effects of C and O in the target. Since finite resolution made it impossible to distinguish scattering from B, C, and O, this was done by adding their contributions in the laboratory frame and then converting the results into a center-of-mass angular distribution using the kinematics appropriate for ^{7}Be + ^{10}B elastic scattering. Figure 2 shows this predicted angular distribution with (solid line) and without (dashed line) a correction for finite angular resolution.

The elastic scattering angular distributions have been predicted using optical model parameters obtained from double folding model calculations convoluting Hartree-Fock density distributions according to the JLM effective interaction [16]. The folded potentials have been renormalized to match the systematics observed in elastic scattering of p-shell nuclei at 9 to 16 MeV/u—including ^{6}Li + ^{12}C [17], ^{7}Li + ^{9}Be, ^{7}Li + ^{12}C [18], ^{7}Li + ^{13}C,

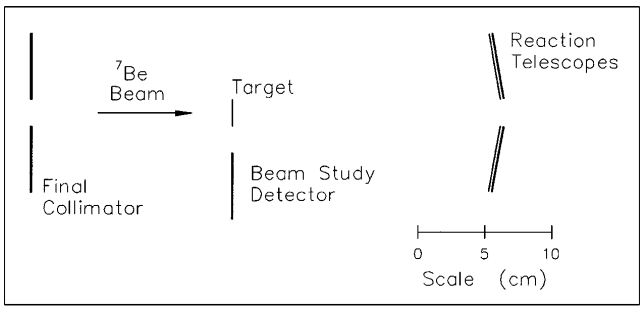

FIG. 1. Target and detector configuration.

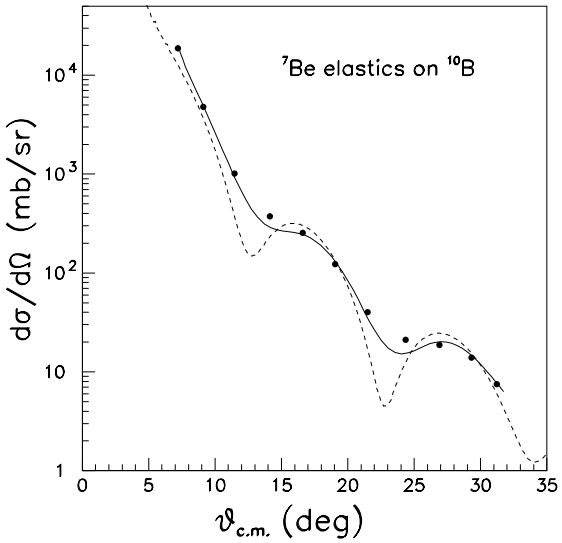

FIG. 2. Observed ^{7}Be elastic scattering angular distribution. Statistical errors are smaller than the plotted data points. The overall normalization uncertainty is $\pm$6.4%. The dashed curve is the predicted angular distribution, summed over the nuclei in the target, while the solid curve shows the same distribution corrected for finite angular resolution.

^{10}B + ^{9}Be [19], ^{13}C + ^{9}Be, and ^{14}N + ^{13}C [20]. In total, eight angular distributions have been analyzed to obtain the renormalization factors needed to fit elastic scattering in this mass region. Since the JLM effective interactions are density dependent, they provide a very good description of the mass dependence of the optical potential. Thus, the renormalization factors have very little dispersion, minimizing the uncertainties due to the choice of optical parameters. Details regarding the optical potentials will be provided in a separate publication [21].

Figure 2 shows good agreement between the expected and observed elastic scattering angular distributions, especially since the calculations do not include contributions from inelastic scattering populating the ^{7}Be or ^{10}B first excited states, neither of which is resolved from the elastic scattering. High resolution elastic scattering studies in this energy region involving ^{7}Li [21] and ^{10}B [19] projectiles imply that these excited states should contribute less than 20% of the total yield observed near the elastic scattering minima, and no more than a few percent near the elastic scattering maxima. It is important to recognize that Fig. 2 does not represent a fit to our measured data. Rather, it is a comparison between the measured absolute cross section for elastic scattering and the predicted absolute cross section from the folding model, with neither adjusted to match the other. Away from the minima, the measured and calculated absolute cross sections agree within 5%. We also used the Monte Carlo simulation to predict the overall energy resolution of the elastic scattering Q-value spectrum integrated over scattering angle, taking the folding model angular distributions as inputs. Again, good agreement was found. These agreements verify that we understand both the target thickness and its nonuniformity.

Figure 3 shows the Q-value spectrum of the outgoing ^{8}B nuclei, while Fig. 4 shows the measured ^{10}B(^{7}Be, ^{8}B)^{9}Be angular distribution for those outgoing ^{8}B nuclei with $Q > -8$ MeV. This corresponds to population of the ^{9}Be ground state, but also includes a small component associated with the ^{9}Be second excited state. For a peripheral transfer reaction like this, ANC's are extracted from the measured cross section by comparison to a distorted-wave Born approximation (DWBA) calculation. In the ^{10}B(^{7}Be, ^{8}B)^{9}Be(g.s.) proton transfer reaction, the experimental cross section is given by

$$\frac{d\sigma}{d\Omega} = \frac{(C^{^{10}\mathrm{B}})^2}{(b^{^{10}\mathrm{B}})^2}\left[\frac{(C^{^{8}\mathrm{B}}_{p_{3/2}})^2}{(b^{^{8}\mathrm{B}}_{p_{3/2}})^2}\,\sigma_{p_{3/2}} + \frac{(C^{^{8}\mathrm{B}}_{p_{1/2}})^2}{(b^{^{8}\mathrm{B}}_{p_{1/2}})^2}\,\sigma_{p_{1/2}}\right]. \quad (1)$$

$\sigma_{p_{3/2}}$ and $\sigma_{p_{1/2}}$ are the calculated DWBA cross sections for proton transfer from the $p_{3/2}$ orbital in ^{10}B to the $p_{3/2}$ and $p_{1/2}$ orbitals in ^{8}B, respectively, and the b's are the asymptotic normalization constants for the single-particle orbitals used in the DWBA. $C^{^{10}\mathrm{B}}$ is the ANC for $^{10}\mathrm{B} \leftrightarrow {}^{9}\mathrm{Be} + p$ [$C^2 = 5.06(46)$ fm^{-1} [19]], and $C^{^{8}\mathrm{B}}_{p_{3/2}}$ and $C^{^{8}\mathrm{B}}_{p_{1/2}}$ are the ANC's for $^{7}\mathrm{Be} + p \leftrightarrow {}^{8}\mathrm{B}$ that, together, determine the S factor for $^{7}\mathrm{Be}(p,\gamma)^{8}\mathrm{B}$ [6]. The parametrization of the DWBA cross section in terms of the ANC's for the two vertices makes their extraction insensitive to the parameters used in the single-particle potential wells [19,20], in contrast to traditional spectroscopic factors. See [19] for additional details.

The DWBA calculations were carried out with the finite-range code PTOLEMY [22], using the full transition operator. The ^{7}Be + ^{10}B distorted waves were calculated with the same folding model optical potential used in the elastic scattering calculations above, while the ^{8}B + ^{9}Be optical potential was derived from a similar folding model calculation. The peripheral nature of the reaction was verified by comparing the results of DWBA calculations while varying the parameters of the single-particle Woods-Saxon potential wells over the ranges $r_0 = 1.0$–1.3 fm and $a = 0.5$–0.7 fm. The predicted cross section integrated over $8° < \theta_{\mathrm{c.m.}} < 30°$ changed by 25%, while the inferred ANC's only changed by $\pm 3.5\%$. The angular resolution of the present experiment is insufficient to distinguish the small difference between the angular distributions of the dominant $p_{3/2} \rightarrow p_{3/2}$ transition and the weak $p_{3/2} \rightarrow p_{1/2}$ transition over the angular region studied. Therefore, we calculated the ^{10}B(^{7}Be, ^{8}B)^{9}Be(g.s.) angular distribution by assuming that $(C^{^{8}\mathrm{B}}_{p_{1/2}})^2/(C^{^{8}\mathrm{B}}_{p_{3/2}})^2 = 0.157$, as given in [23]. Figure 4 shows that our observed angular distribution is in good agreement with the predicted shape, normalized to the cross section that we determine from the Q-value fit described below.

To obtain the most precise determination of the ^{8}B ANC's, we have fit the Q-value spectrum shown in Fig. 3 to obtain the total ^{10}B(^{7}Be, ^{8}B)^{9}Be(g.s.) cross section. The predicted angular distribution of Fig. 4 was input to the Monte Carlo simulation—which calculated the shape,

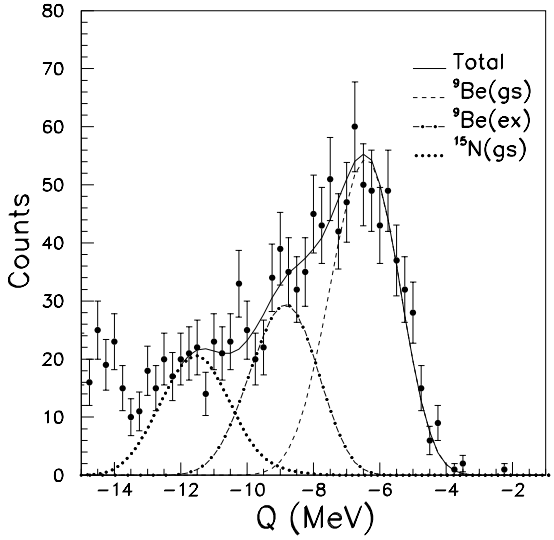

FIG. 3. Q-value spectrum of the outgoing ^{8}B nuclei. The curves are Monte Carlo simulations of the ^{10}B(^{7}Be, ^{8}B)^{9}Be reaction, populating the ^{9}Be ground and second excited states, and the ^{16}O(^{7}Be, ^{8}B)^{15}N(g.s.) reaction. The solid curve is a fit over the region -12 MeV $< Q < -4$ MeV.

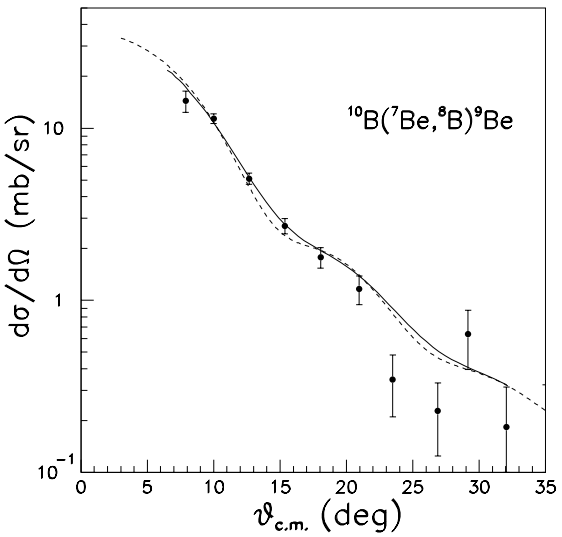

FIG. 4. Measured ^{10}B(^{7}Be, ^{8}B)^{9}Be angular distribution for those events in Fig. 3 that have $Q > -8$ MeV. The dashed curve shows the predicted angular distribution, normalized to the cross section inferred from the Q-value fit, while the solid curve is corrected for finite angular resolution.

location, and magnitude of the (^{7}Be, ^{8}B) Q-value peak. Angular distributions were also calculated using similar techniques for reactions populating the ^{9}Be second excited state and the ^{15}N ground state from the ^{16}O in the target, then input to the Monte Carlo simulation to determine their corresponding Q-value peak shapes. A three-parameter χ^2 minimization provided the best fit to the measured Q-value spectrum over the range -12 MeV $< Q < -4$ MeV and determined the absolute cross sections for populating the ^{9}Be ground and second excited states. Figure 3 also shows ^{8}B yield beyond -12 MeV from population of higher excited states in ^{9}Be and reactions off the ^{12}C in the target. These states were not included in the Q-value fit as they have a negligible impact on the absolute cross sections of interest. The Q-value fit gives $\sigma = 1.40 \pm 0.13$ mb for the ground state cross section. This gives $C^2_{p_{3/2}} = 0.398 \pm 0.062$ fm^{-1} for ^{8}B. The contributions to the uncertainties are: statistics (4.0%), absolute normalization of the measured cross section (6.4%), inputs to the Monte Carlo simulation (2.4%), inputs to the DWBA (10%), and knowledge of the ^{10}B ANC (9%). The ratio of the measured cross sections for the two ^{9}Be states is $\sigma_{\mathrm{exc}}/\sigma_{\mathrm{g.s.}} = 0.52 \pm 0.05$, consistent with the expectation of $\sim$0.5 from DWBA calculations with shell model wave functions [24].

The relation between the ^{8}B ANC's and $S_{17}(0)$ was derived in [6], which found

$$S_{17}(0) = \frac{38.6\ \mathrm{eV\,b}}{\mathrm{fm}^{-1}}\left[(C^{^8\mathrm{B}}_{p_{3/2}})^2 + (C^{^8\mathrm{B}}_{p_{1/2}})^2\right]. \qquad (2)$$

Thus, we conclude that $S_{17}(0) = 17.8 \pm 2.8$ eV b for ^{7}Be$(p, \gamma)^{8}$B. This is in excellent agreement with the results obtained from the three smaller direct measurements of the ^{7}Be$(p, \gamma)^{8}$B cross section [3–5] and nearly 3σ below the two larger direct measurements [1,2], and has been found using a procedure with completely independent systematic effects from those present in the ^{7}Be radioactive target experiments. This agreement provides independent confirmation of the procedure in [5], which chose to calculate $S_{17}(0)$ based on a weighted mean of the three smaller direct measurements alone. The uncertainty in the ^{8}B ANC's found here will be reduced slightly after the analysis of a measurement of the ^{10}B ANC using the ^{9}Be(^{3}He, d)^{10}B reaction has been completed. Measurements of the (^{7}Be, ^{8}B) reaction from other targets could further reduce the uncertainty in the ^{8}B ANC's, and hence the determination of $S_{17}(0)$, in the future.

We would like to thank P. Svihla for assistance with the ^{10}B target fabrication. This work was supported in part by the U.S. Department of Energy under Grant No. DE-FG03-93ER40773 and by the Robert A. Welch Foundation.

[1] P. D. Parker, Phys. Rev. **150**, 851 (1966).
[2] R. W. Kavanagh *et al.*, Bull. Am. Phys. Soc. **14**, 1209 (1969).
[3] F. J. Vaughn *et al.*, Phys. Rev. C **2**, 1657 (1970).
[4] B. W. Filippone *et al.*, Phys. Rev. Lett. **50**, 412 (1983); Phys. Rev. C **28**, 2222 (1983).
[5] F. Hammache *et al.*, Phys. Rev. Lett. **80**, 928 (1998).
[6] H. M. Xu *et al.*, Phys. Rev. Lett. **73**, 2027 (1994).
[7] P. Descouvemont and D. Baye, Nucl. Phys. **A567**, 341 (1994).
[8] A. Csoto, Phys. Lett. B **394**, 247 (1997).
[9] E. G. Adelberger *et al.*, Rev. Mod. Phys. **70**, 1265 (1998).
[10] T. Motobayashi *et al.*, Phys. Rev. Lett. **73**, 2680 (1994).
[11] C. A. Gagliardi *et al.*, Phys. Rev. C **59**, 1149 (1999).
[12] W. Liu *et al.*, Phys. Rev. Lett. **77**, 611 (1996).
[13] C. A. Gagliardi *et al.*, Phys. Rev. Lett. **80**, 421 (1998).
[14] R. E. Tribble, R. H. Burch, and C. A. Gagliardi, Nucl. Instrum. Methods Phys. Res., Sect. A **285**, 441 (1989).
[15] R. E. Tribble, C. A. Gagliardi, and W. Liu, Nucl. Instrum. Methods Phys. Res., Sect. B **56–57**, 956 (1991).
[16] J. P. Jeukenne, A. Lejeune, and C. Mahaux, Phys. Rev. C **16**, 80 (1977).
[17] P. Schwandt *et al.*, Phys. Rev. C **24**, 1522 (1981).
[18] A. F. Zeller *et al.*, Phys. Rev. C **22**, 1534 (1980).
[19] A. M. Mukhamedzhanov *et al.*, Phys. Rev. C **56**, 1302 (1997).
[20] L. Trache *et al.*, Phys. Rev. C **58**, 2715 (1998).
[21] L. Trache *et al.* (unpublished).
[22] M. Rhoades-Brown, M. McFarlane, and S. Pieper, Phys. Rev. C **21**, 2417 (1980); **21**, 2436 (1980).
[23] A. M. Mukhamedzhanov and N. K. Timofeyuk, Sov. J. Nucl. Phys. **51**, 431 (1990).
[24] S. Cohen and D. Kurath, Nucl. Phys. **73**, 1 (1965).